CLAS-NOTE 2007-007

CLAS12 pre-shower readout system

G. Asryan, H. Voskanyan
YerPhI

S. Stepanyan
JLAB

Abstract

CLAS12 forward electromagnetic calorimeter will consist of the existing CLAS electromagnetic calorimeter and a pre-shower calorimeter with finer segmentation of the readout planes. In the pre-shower, light from scintillator to a photo detector will be transported via green wave shifting fibers embedded in the surface of the scintillator strip. In this report the light yield measurements for different configurations of light readout system of the pre-shower are presented. Final selection of the scintillator type, wave shifting fiber, and the PMT for the main detector will be based on the performance, photo-electron statistics, and the price. Based on the results of measurements and the available price estimates, we conclude that the best choice for the pre-shower components will be: the FNAL extruded scintillator, the KURARAY 1 mm diameter, single clad wave-length shifting fiber (Y11), and the HAMAMATSU R6095 PMT, selected to have quantum efficiency $> 16\%$ at 500 nm. It should be notted that by the performance and price, extruded scintillators from Amcrys-Plast, Kharkov (Ukraine), wave-length shifting fibers G91A from BICRON and the HAMAMATSU PMT R1450, selected to have $> 18\%$ quantum efficiency at 500 nm, were not too far from the best choice set and generally meet the requirements for the pre-shower.

1 Introduction

In the current configuration, CLAS forward electromagnetic calorimeter (EC) [1] will not be able to resolve two photon clusters from a high energy

(> 6 GeV) π^0 decay due to close proximity of two photon clusters on the EC plane, see Fig.1. To resolve closely located hits, a finer granularity of the shower energy measurements in the transverse plane is required [2]. CLAS12 detector will be instrumented with a pre-shower calorimeter. The geometry of the pre-shower will be similar to the geometry of EC. It will consist of alternating layers of lead and scintillators in almost equilateral triangular shape. Scintillator layers will consist of about 4.5 cm wide scintillator strips. In each following layer, scintillator strips will be parallel to one the sides of the triangle (rotated $\sim 120^o$ relative to the orientation of the previous layer), those forming three stereo readout system. The light from the scintillator strips will be read out via 1 mm diameter green wave shifting fibers (WLSF), glued inside straight grooves along the scintillator strip on the surface of a strip, see Fig.2.

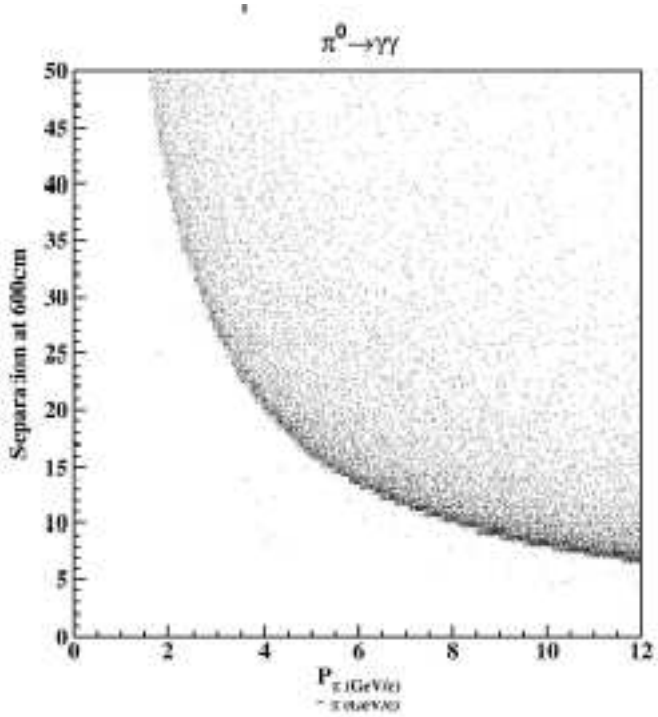

Figure 1: Distance between two photons on a plane located at 600 cm away from the target as a function of π^0 momentum. Transverse segmentation of the current calorimeter is about 10 cm

The scintillator light readout systems with embedded fibers are well known.

The technique proposed for the pre-shower was tested and showed very good results, see [3]. This technique was used, for example, in the MINOS FAR detector [4] and many other "tile" calorimeters. In this report we present results of the test measurements of several scintillator-WLSF-PMT systems. The goal of this study was to select an optimal light collection system for the CLAS12 pre-shower, based on the light yield and the price. These work was performed as a part of the R&D for the CLAS12 pre-shower.

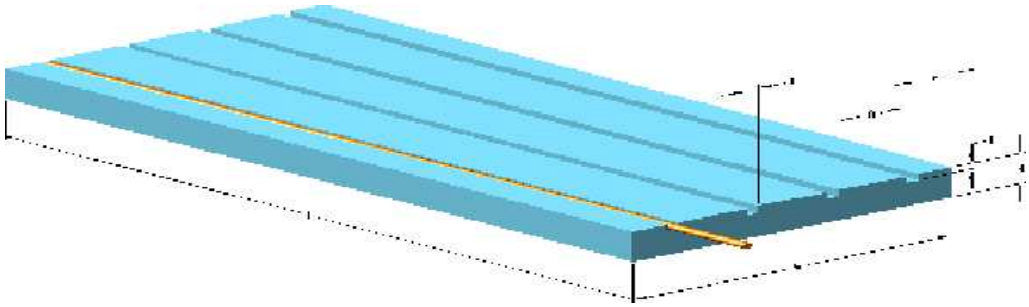

Figure 2: Scintillator strip with four grooves on the surface for the wave shifting fiber readout.

2 Pre-shower components

For this test measurements, several different types of scintillator material, wave shifting fibers (single and multi clad), and PMTs were purchased from different vendors, see Table 1. Scintillators from Fermi lab and Amcrys-Plast, Kharkov (Ukraine), were produced using the extrusion method [5, 6] and grooves were made during the extrusion. (The number of grooves will not effect on the final price.) These strips had a reflective coating on surfaces (excluding the inside surface of of grooves). Scintillator strips from ELJEN Technologies were cut from prepared bulk material using a diamond cutting tools and the grooves were machined. These strips did not have any reflective cover. ELJEN scintillator strips without grooves were obtained to

make grooves in-house, using the method implemented in [3], to save some cost. The HAMAMATSU R1450-13 PMT was selected with Sk> 120 for high quantum efficiency (QE) at 500 nm, QE > 18%. The R6095 was selected with Sk> 100 for QE > 16% at 500 nm, see Fig. 3. The KURARAY 1.5 mm and 2 mm diameter Y11 fibers were used to study overall light yield dependence on the fiber diameter. Light yield measurements were carried out not for every possible combinations of the scintillator-WLSF-PMT, but enough measurements were made to be able to determine the best combination.

PMT	Type	Photo cathode	# of stages
HAMAMATSU	R7899EG	25 mm	10
	R1450-13	19 mm	10
	R6095	28mm	11
ElectronTubes	9124B	30mm	11
PHOTONIS	XP1912	19mm	10
	XP2802	19mm	10
WLS fibers	Type	Diameter	Cladding
KURARAY	Y11	2mm	Single
	Y11	1.5mm	Single
	Y11	1mm	Single
	Y11	1mm	Multi
BICRON	BC-91A	1mm	Single
	BC-92	1mm	Single
Scintillators	Type	Cross section	# of grooves
ELJEN Tech.	EJ-204	3×1 cm^2	4
	EJ-204	3×1 cm^2	No grooves
FNAL	MINOS	4×1 cm^2	1
Amcrys-Plast, Kharkov		2.6×1 cm^2	2
		2.6×1 cm^2	3

Table 1: Pre-shower readout components used in the test.

3 Setup

Measurements were performed in the semi-clean room in the EEL building

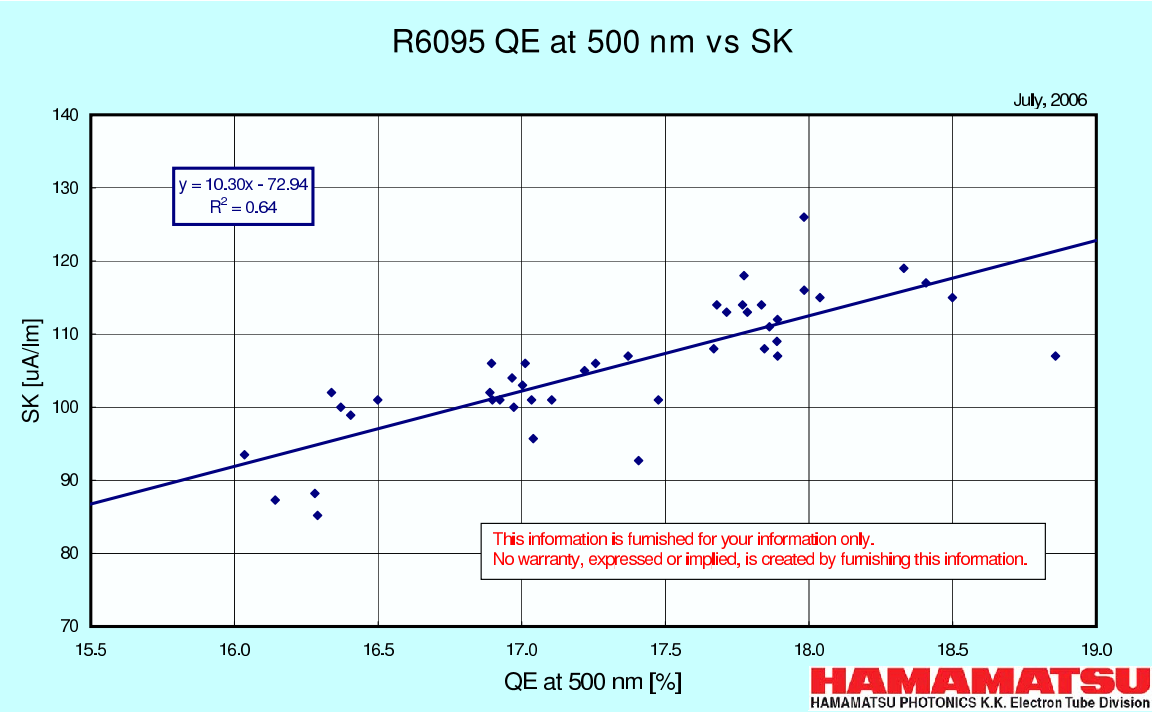

Figure 3: Sk vs. QE for the HAMAMATSU R6095 PMT.

at JLAB, using 4 meters long dark box, see Fig.4. The box was instrumented with a moving cart, but for this set of measurements position dependence of the light yield was not studied and the cart was not used. In Fig.5, a schematic view of the setup is shown. Scintillator strips with fibers were secured inside the box. The trigger PMT was attached directly to the end of the scintillator strip through acrylic light guide. For the scintillator-light guide and the light guide-PMT connections BICRON BC-630 optical grease was used.

WLS fibers were glued inside grooves using Dymax UV curable optical glue OP-52. Fibers were extended about 40 cm from the end of the scintillator in order to connect to the photo cathode of a test PMT. The test PMT was installed inside a plastic housing, a tube with μ-metal shield inside. The housing tube had two end-cups, one with connectors for HV and signal cables

Figure 4: Picture of the dark box. Moving cart is mounted on rails

and the another with adapter for the fiber connection [8]. To secure the fiber on the photo cathode of the test PMT, several plastic adapters were built with thin metallic tubes as an inserts. The inner diameter of tubes were chosen to have a tight fit for the fibers. The tubes were aligned along the axis of the PMT and were guiding the fibers in the direction perpendicular to the photo cathode. BICRON EC-630 optical grease was used between the fiber and the photo cathode for good optical contact.

Readout electronics of the system consisted of the LeCroy 1881M ADC and the Philips 704 discriminator. As a gate for the ADC, discriminated pulse from the trigger PMT was used. Signals of the test and the trigger PMTs were delayed and connected to the ADC inputs, see Fig.5. The ADC information was read out using the standard CLAS DAQ software. For each setting, ADC values were written out to a single file. Then the information

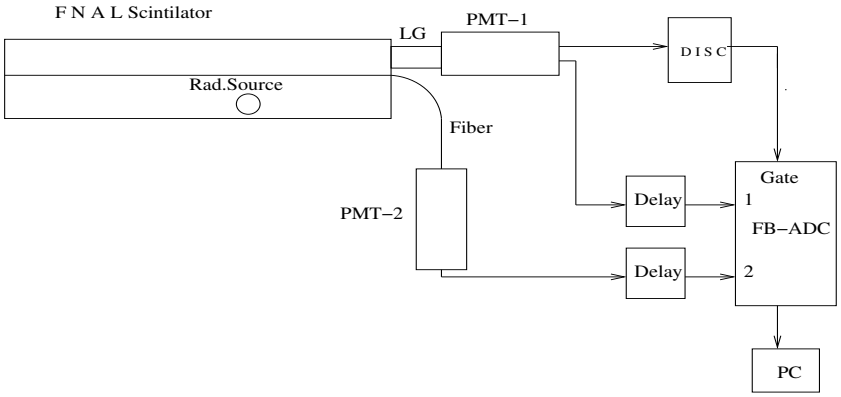

Figure 5: Schematic view of the setup for light yield measurements

was copied into HBOOK Ntuple [9]. Analysis of the data were performed in PAW [10].

4 Measurements and analysis

Most of the measurements were carried out with ^{90}Sr radioactive source (β, $E = 0.546$ MeV) positioned on top of the scintillator. Strontium β decay produces ^{90}Y which also has a β decay with maximum energy of 2.28 MeV. So, the maximum energy deposited in the scintillator was assumed to be ~ 2 MeV.

The systematic uncertainties in the measurements were estimated by checking the reproducibility of the photo-electron yields for the same combination of the scintillator-fiber-PMT, measured at different settings. In Fig. 6 ADC distributions of 9124B PMT for three different measurements is shown. In all three measurements the trigger PMT optical connection and the location of the source were the same. The fiber was disconnected and then connected for different measurements. In this particular case the difference is less then 2.5%. Similar measuremnts were carried at different HV settings of the test PMT (different gains) and for different optical connection of the trigger PMT to the scintillator. Overall the reproducibility of measurements was found to be $< 10\%$.

Additional measurements using cosmic muons and ^{207}Bi source were performed to check obtained results on photo electron statistics.

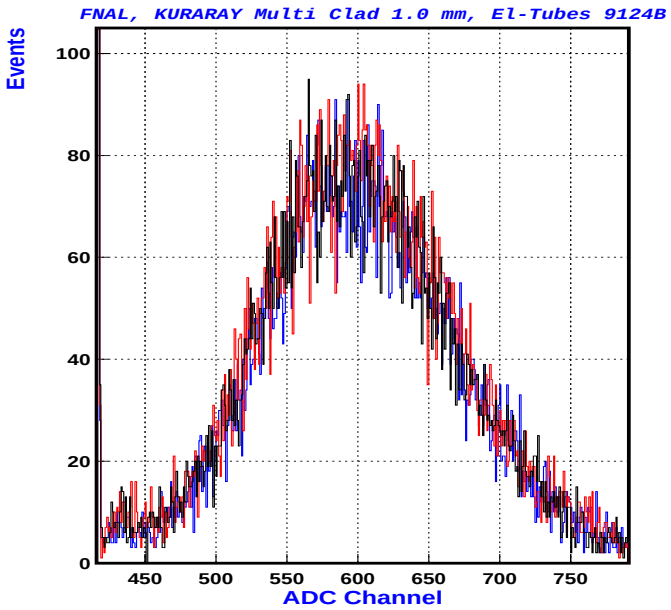

Figure 6: ADC distributions of ElectronTubes 9124B PMT for three different measurements.

4.1 Determination of the number of photo-electrons

For the analysis of photo-electron statistics, the method developed in [7] was used. Each ADC spectrum was fitted with a sum of the Puassonian probabilities, $P_i(n_{pe})$, of the number of photoelectrons convoluted with a Gaussian function, $C_i(n_{ch})$, representing the ADC distribution for a given number of photoelectrons:

$$A = c \cdot \sum_i P_i(n_{pe}) \times C_i(n_{ch}) \quad (1)$$

$$P_i(n_{pe}) = \frac{n_{pe}^i \cdot e^{-n_{pe}}}{i!} \quad (2)$$

$$C_i(n_{ch}) = \frac{1}{\sigma_1 \cdot \sqrt{i}} \cdot e^{-(\frac{n_{ch}-(a_1+(i-1)\cdot a_0)}{\sigma_1 \cdot \sqrt{2i}})^2} \quad (3)$$

In Eq.(1), summation goes over the possible number of photoelectrons in the spectrum, i. Coefficient c is for the overall normalization, n_{pe} is the aver-

age number of photoelectrons. In Eq.(3) n_{ch} is the pedestal subtracted ADC channel number. Parameters a_1 and σ_1 are the position and the standard deviation of the single photo-electron peak in the units of ADC channel. a_0 is the distance between two adjacent photo-electron peaks in the units of ADC channels (not necessary to be equal to a_1). The fit parameters were c, n_{pe}, and a_0.

The parameters a_1 and σ_1 were defined from fits to a single photo-electron distributions of the test PMTs using a Gaussian function. The single photo-electron peak was identified by decreasing the amount of light going to the photo cathode. A single peak in the spectrum above the pedestal was identified as a single photo-electron peak, when further decrease of the light will only change the hight of the peak but not the position. On the left graph of Fig. 7, the ADC distributions of XP2802 PMT is shown for different distances between the fiber end and the photo-cathode (spectra are normalized). With increase of the distance (with decrease of the amount of light) the peak at ADC channel #433 and the left shoulder of that peak stay unchanged, while the number of events on the right side, higher ADC channels, is decreasing. The peak was attributed to the single photo-electron distribution of the XP2802 and was fitted with Gaussian function in order to extract the a_1 and σ_1. This procedure was applied to all tested PMTs at every HV settings used in the measurements. As an example, the ADC distribution of the HAMAMATSU R6095 PMT, corresponding to the single photo-electron is shown on the right graph of Fig.7. A fit to this distribution with a sum of two Gaussian functions (corresponding to the pedestal and the single photo-electron peak) resulted to $a_1 = 14.6$ and $\sigma_1 = 9.06$.

4.2 Determination of the absolute light yield

Since the measurements were carried out with β-source, ADC distribution of the test PMT will correspond to the part of the β spectrum that was selected by the trigger PMT. That selection depends on the optical connection between the trigger PMT and the scintillator, on the trigger PMT HV, and on the discriminator threshold. In order to avoid systematic uncertainties due to a continuous energy spectrum, the photo-electron yields for different combinations, corresponding to the end point energy ($\sim$ 2 MeV) were compared. For this, the test PMT spectra were fitted with Eq.(1) for different ranges of the trigger PMT ADC distribution, see Fig. 8. With increase of the trigger PMT ADC channel number, the average number of

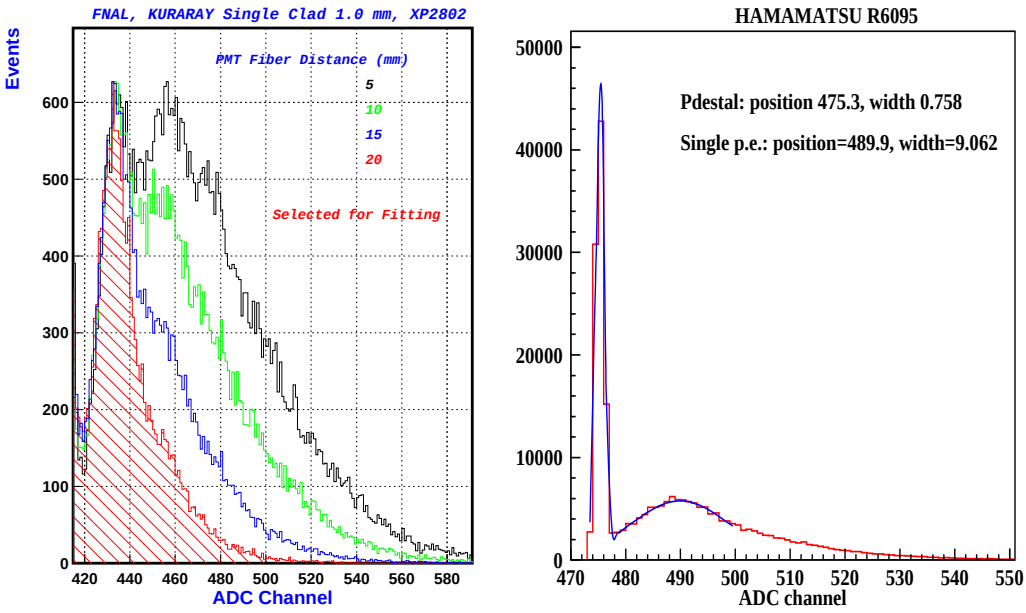

Figure 7: On the left is the ADC distribution of XP2802 PMT corresponding to a few and single photoelectrons. On the right fit to the single photo-electron distribution of the HAMAMATSU R6095 PMT. Fit was done using a sum of two Gaussians, one for the ADC pedestal and the second one is for the single photo-electron distributions.

photoelectrons in the test PMT, n_{pe}, should increase and one expects it will reach to a maximum value and will stay constant at the end of the spectrum. In Fig. 9, fits to the ADC distributions of the HAMAMATSU R7899EG and R6095 PMTs, corresponding to the trigger PMT ADC range from 550 to 600 are presented. The dependence of the n_{pe} on the trigger PMT ADC channel is shown in Fig. 10. Closed squares are n_{pe}'s for R7899EG, the open squares are for R6095. The solid line curve is the χ^2 distribution for the fit to the spectra of R7899EG. As one would expect number of photoelectrons increases with increase of the trigger PMT ADC channel number and at the end starts to flattened out (clearly seen for R7899EG). At the end points the energy deposition in the scintillator is about $\sim$ 2 MeV. Such analysis were performed for every measured spectrum. The number of photoelectrons at the end point were taken as a light yield corresponding $\sim$ 2 MeV energy

deposition.

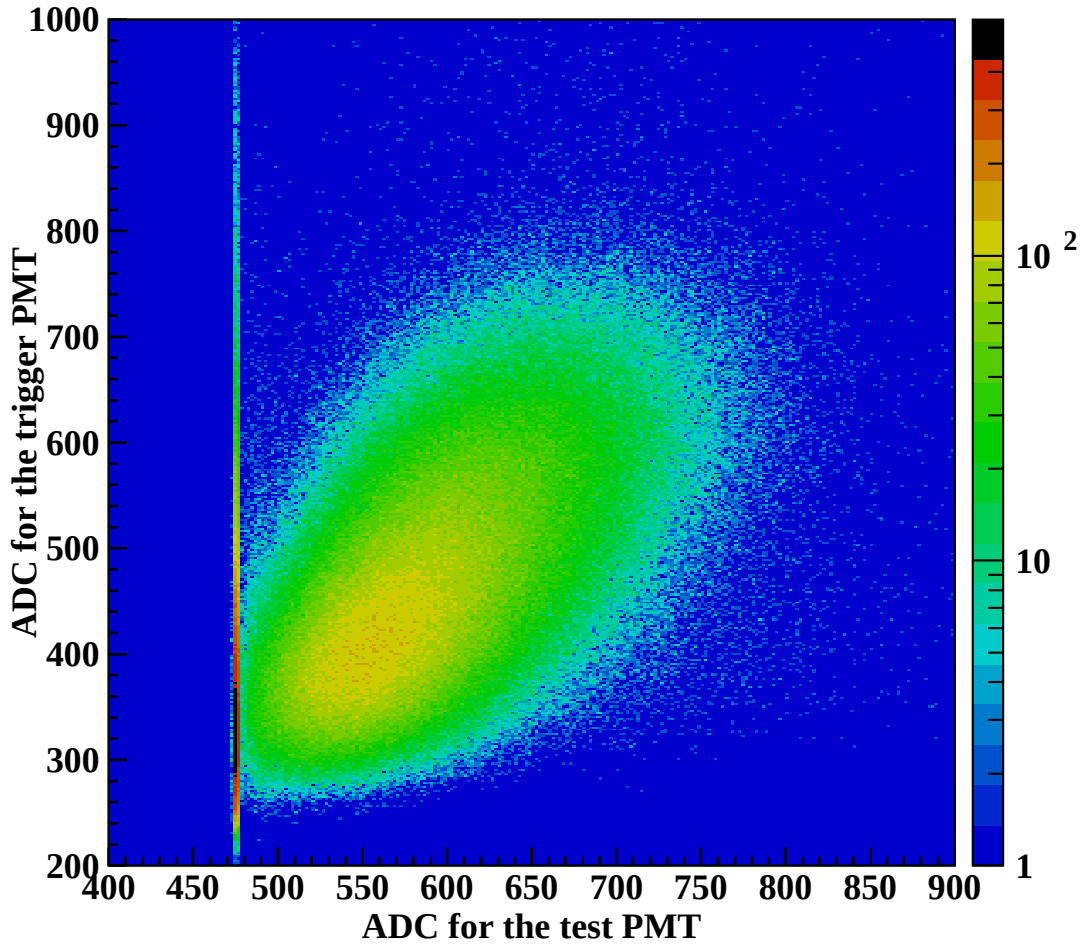

Figure 8: ADC spectra of the trigger and test PMTs. Test PMT ADC distributions for different slices of the trigger PMT ADC were fitted to get photo-electron statistics.

5 Light yield with single fiber readout

Distributions presented in Fig.10 were obtained for several different combinations of scintillator-WLSF-PMT. In Fig. 11, light yield for different

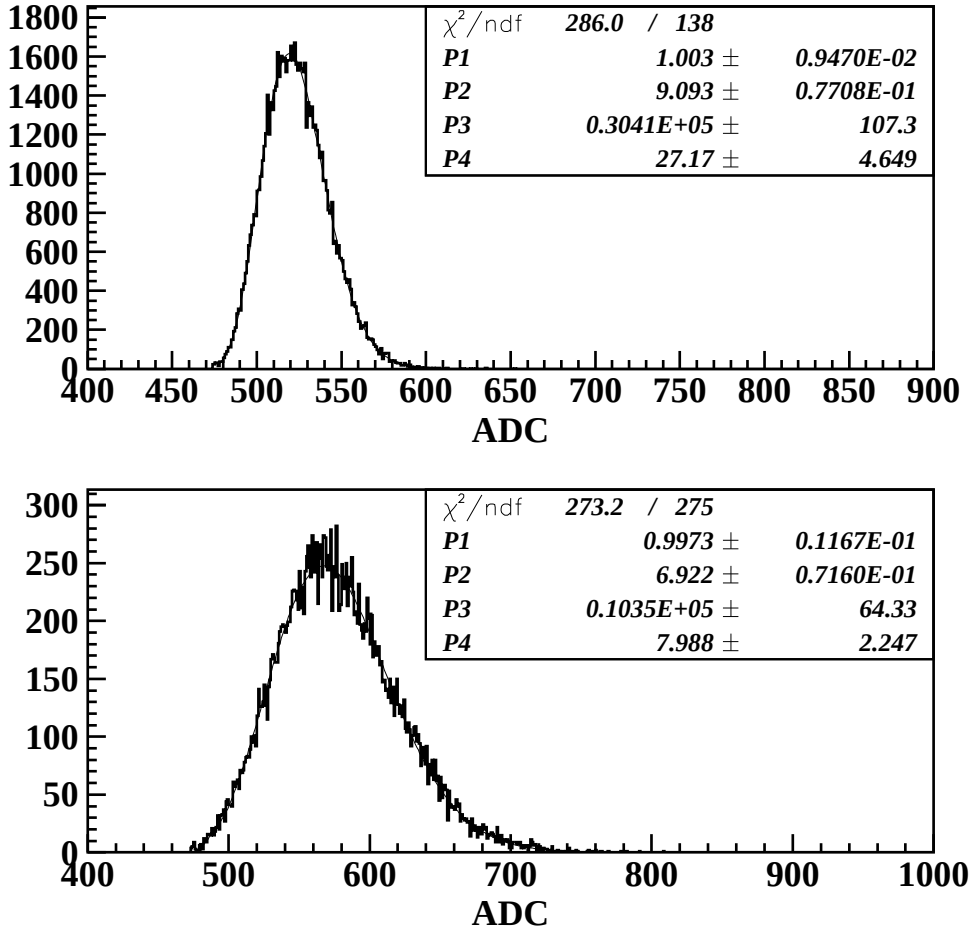

Figure 9: Fit to the ADC spectra of the HAMAMATSU R7899EG and R6095 PMTs with Eq.(2). Spectra correspond to the trigger PMT ADC channels 550 to 600.

PMTs are shown as a function of the trigger PMT ADC channel. Measurements for different PMTs were performed with the same FNAL scintillator and the single clad 1 mm diameter Y11 WLS fiber. All the fits show flattening at the end of the spectrum of the trigger PMT. The number of photoelectrons corresponding to ~ 2 MeV energy deposition for all measured PMTs are presented in Table 2.

Clearly, the HAMAMATSU R7899EG (green extended photocathode)

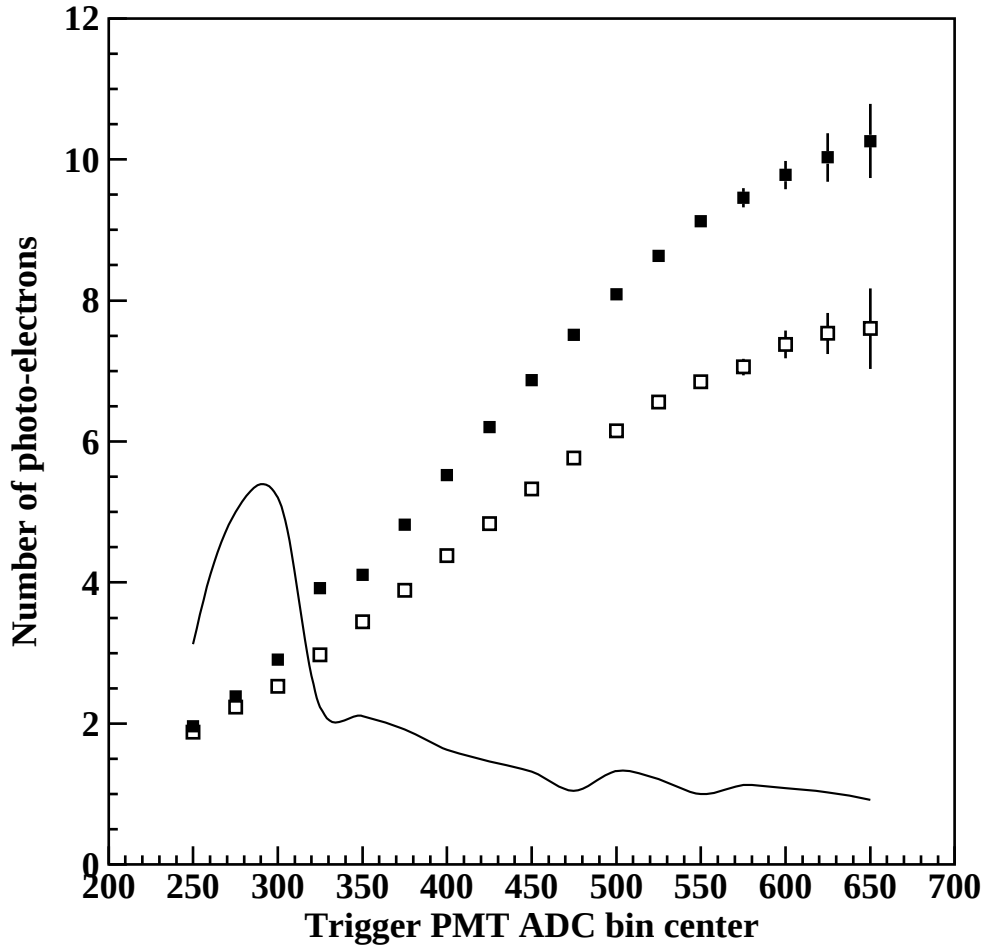

Figure 10: Dependence of the n_{pe} on the trigger PMT ADC channel. On the figure closed squares are the n_{pe} for R7899EG, the open squares are for R6095. The solid line curve is the χ^2 distribution for the fit to the spectra of R7899EG.

has the highest light yield. The HAMAMATSU R6095, selected for $QE >$ 16% at 500 nm, yielded $\sim$ 26% less photoelectrons. Other PMTs, the PHOTONIS XP2902, the ElectronTubes 9124B, and the HAMAMATSU R1450, that was also selected to have high QE at 500 nm, did not perform as well as the first two.

Measurements with different scintillator types, the FNAL and Kharkov extruded, and the ELJEN tech. EJ204, were performed using R6095 PMT. All the strips had 1 mm, single clad Y11 fiber glued in the groove on the

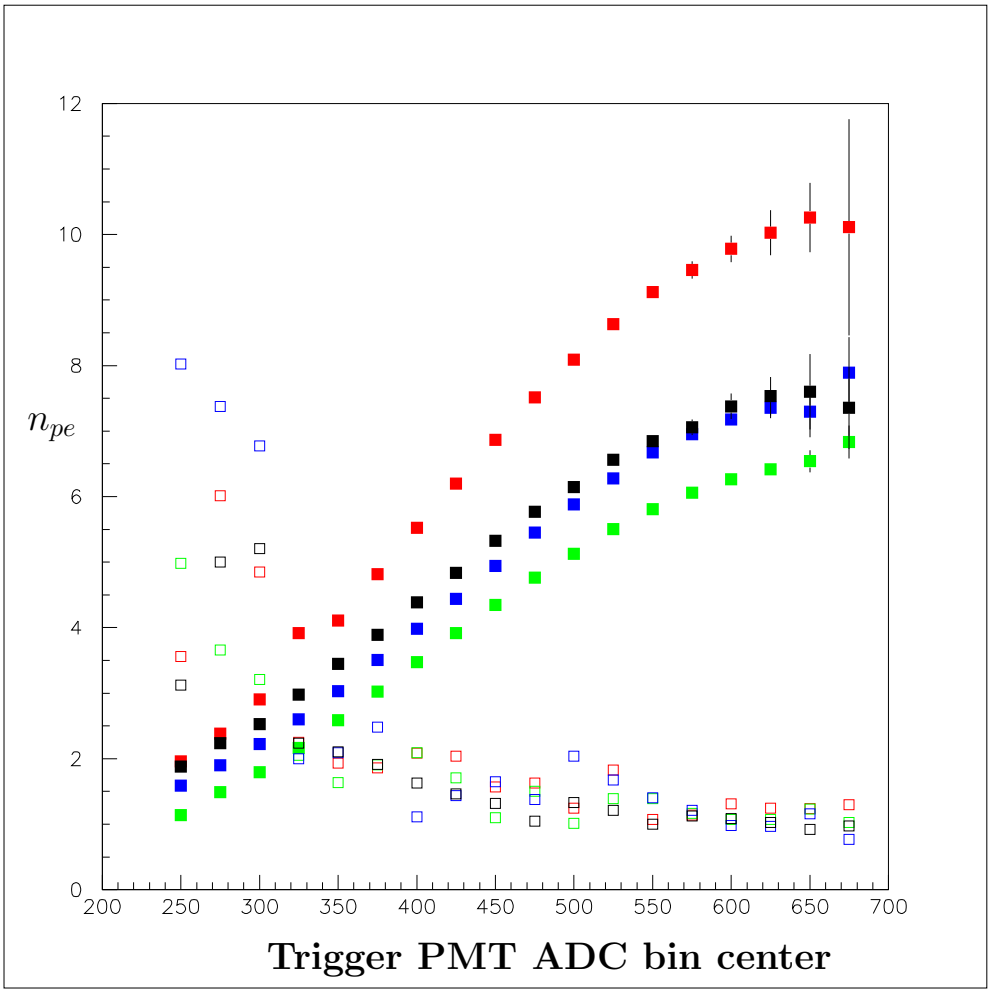

Figure 11: Dependence of the n_{pe}'s on the trigger PMT ADC channel. Closed squares are the n_{pe}'s for R7899EG (red), R6095 (black), XP2802 (blue), and R1450 (green). The open squares the χ^2 distributions for the fits (in the same color codding).

surface of the strip. The EJ204 did not have reflective coating, therefore two measurements with and without wrapping were done for that scintillator. Obtained results are presented in Table 3 and are shown in Fig.12. The FNAL extruded scintillator showed the highest light yield.

Dependence of the light yield on the WLS fiber type was studied as well. Different type and diameter fibers were glued into the FNAL scintillator

PMT	R7899EG	R6095	XP2802	R1450	9124B
n_{pe}	10.3	7.6	7.3	6.5	4.7
$\sigma_{n_{pe}}$	0.53	0.57	0.39	0.17	0.14
χ^2	1.7	0.92	1.16	1.23	0.7

Table 2: Number of photoelectrons for different PMTs corresponding to 2 MeV energy deposition in the FNAL extruded scintillator with one groove. Readout with 1mm diameter, single clad Y11 WLS fiber.

	FNAL	ELJEN	ELJEN wrapped	Kharkov
n_{pe}	7.6	2.5	5.7	6.8
$\sigma_{n_{pe}}$	0.57	0.55	0.33	0.23
χ^2	0.92	1.08	1.1	1.02

Table 3: Number of photoelectrons for 2 MeV energy deposition in different scintillator strips. Readout was with 1 mm, single clad Y11 WLS fiber and R6095 PMT.

strip and the photo-electron statistics was measured with the HAMAMATSU R7899EG PMT. The relative light yield for different fibers is presented in Fig.13. Light yield for the BICRON G92 fiber is not presented, it was too low (not a surprise since G92 is designed to have fast response time and has small attenuation length).

The number of photoelectrons increases with the diameter of the fiber, 1.5 mm fiber has $\sim$ 25% more light than 1 mm diameter fiber and 2 mm fiber has $\sim$ 40% more light. The light yield is also higher for a multi-clad fiber compare to a single clad by about 20%. Bicron G91A 1 mm diameter, single clad fiber has about 10% less light yield than KURARAY 1.0 mm, single clad Y11.

5.1 More measurements

Additional measurements had been performed in order to check the systematics of the results. The same scintillator-WLSfiber-PMT combinations were measured at several settings, to check the reproducibility. It was found that within few % results of different measurements are consistent. One of the

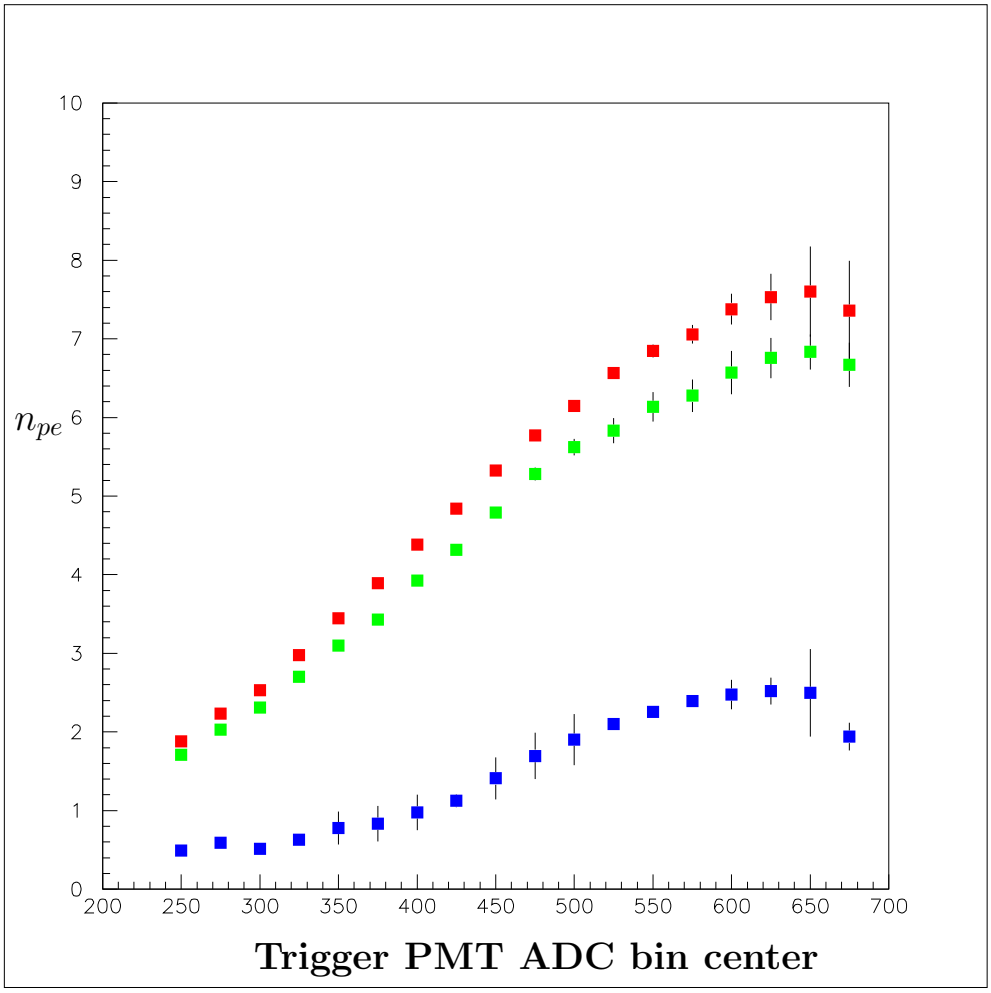

Figure 12: Dependence of the n_{pe}'s on the trigger PMT ADC channel. Closed squares are the n_{pe}'s for the FNAL extruded scintillator strip (red), Kharkov extruded scintillator strip (green), and ELJEN diamond cut strip (blue). Note that the FNAL and Kharkov scintillator strips have reflective coating, while ELJEN was only wrapped in the aluminized mylar.

major sources of the error is the determination of the single photo-electron peak position and the Gaussian width for a given PMT. Measurements with different voltages for the same PMT were performed to study errors due to the single photo-electron peak position and width determination. In Fig. 14, dependences of the number of photoelectrons on the trigger PMT ADC bin center for different HV settings on R6095 are shown, closed squares. The green points are at $HV = 900$ V, the red points at $HV = 850$ V, and the blue

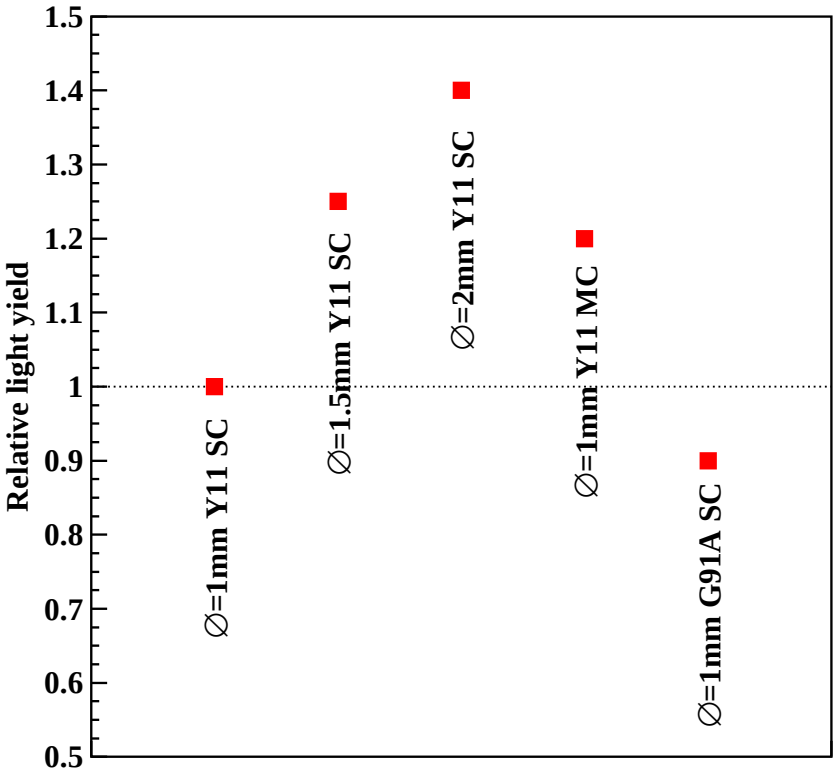

Figure 13: Light yield for different WLS fiber readout relative to 1mm diameter, single clad Y11 fiber. In all cases the fibers were glued to the FNAL extruded fiber and the HAMAMATSU R7899 PMT was used for the readout.

points at $HV = 800$ V. The open squares correspond to the χ^2 distributions of the fits. The maximum difference in the bin centered at 650 is $< 10\%$.

Measurement of the light yield for R6095 PMT with FNAL scintillator and 1 mm diameter single clad Y11 fiber with cosmic muons was performed to check the absolute light yield. As a gate for ADC the coincidence of the trigger PMT and the scintillator counter positioned above the scintillator strip was used. The counter had 1 cm thick, 1.5×4 cm^2 scintillator. Correlation between the trigger and test PMT ADC spectra is shown in Fig. 15. Fit to the test PMT spectrum, selected with a cut on the trigger PMT ADC in the range from 700 to 1500, is presented in Fig. 16. The fit yielded to ~ 9 photoelectrons. There is a difference of 20% compared to the number

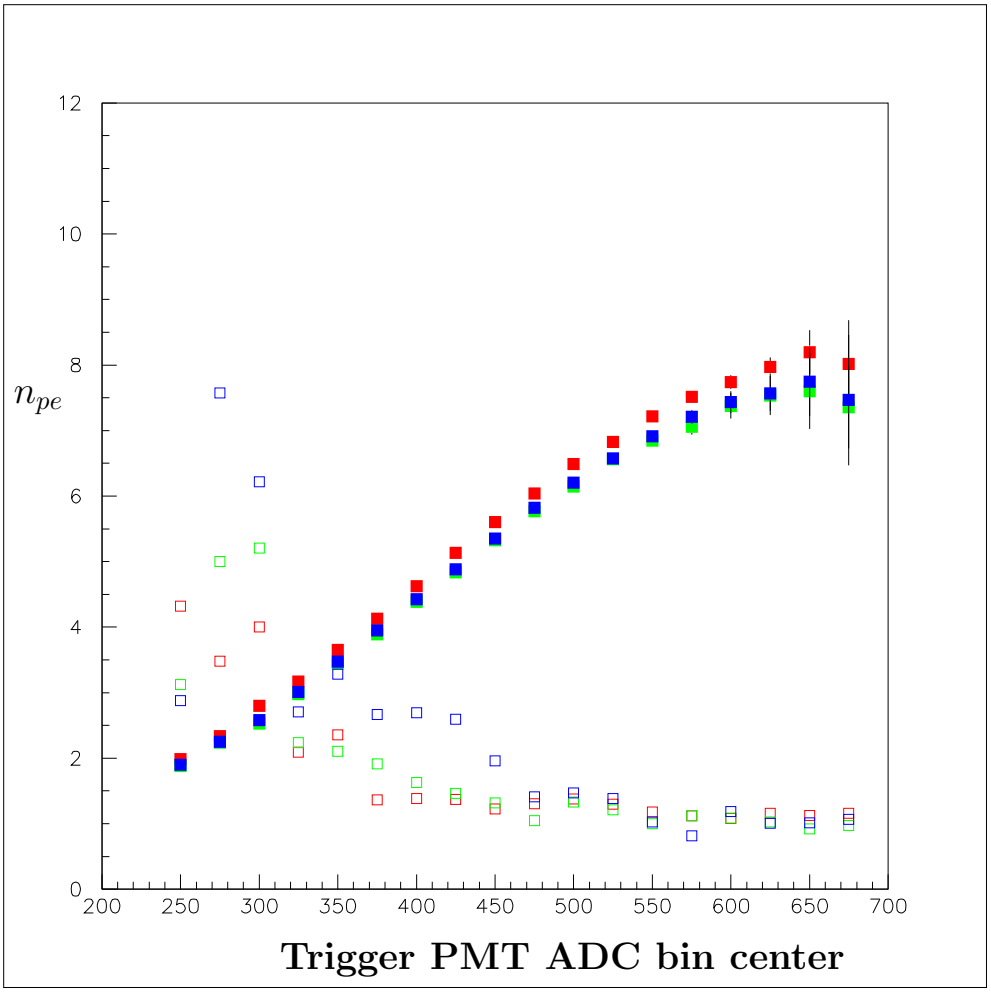

Figure 14: Light yield for the HAMAMATSU R6095 PMT operated at different HV settings. The blue squares correspond to $HV = 800$ V, the read squares are at $HV = 850$ V, and the green squares $HV = 900$ V. The open squares correspond to the χ^2 distributions of the fits.

of photoelectrons obtained with ^{90}Sr source ($\sim$ 2 MeV energy deposition). This difference can be explained by the fact that in the cosmic setup the average path of particles is > 1 cm. More precise measurements of the absolute photo-electron yield will be done with a mini-prototype.

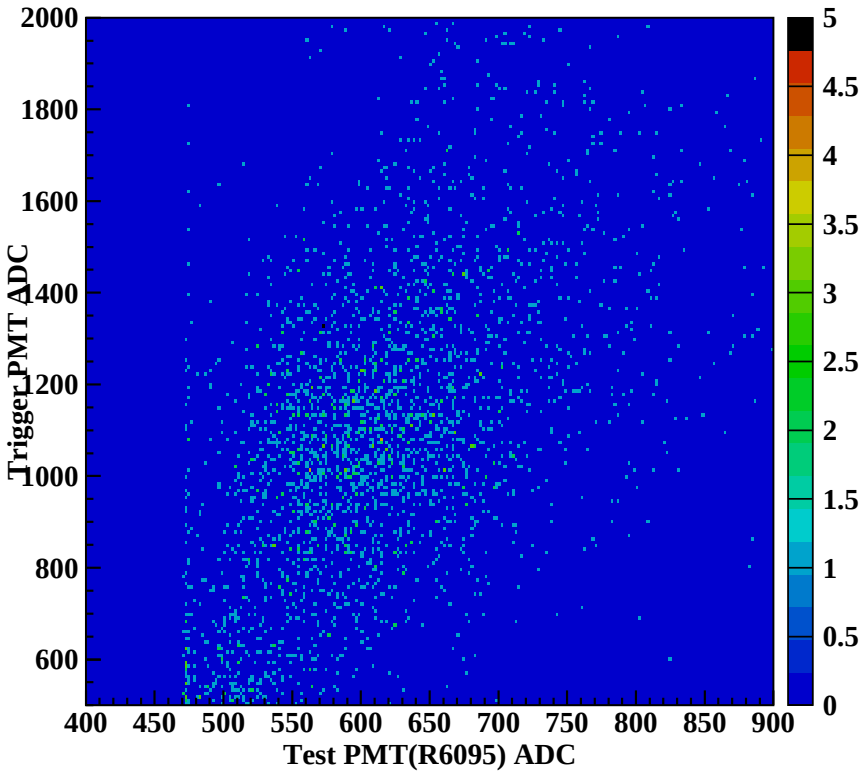

Figure 15: ADC spectra of the trigger and test PMTs for cosmic muons. Test PMT was R6095 operated at 900 V. FNAL scintillator with one 1mm, single clad Y11 WLS fiber was used.

6 Multiple fiber readout

In the final design of the pre-shower, each scintillator strip will be read out with three WLS green fibers embedded in the grooves on the surface of the scintillator strip. To estimate expected light yield for three fiber readout, the Amcrys-Plast, Kharkov, extruded scintillator strips with three grooves were used with KURARAY 1 mm diameter, single clad Y11 fibers. In Fig. 17, the light yield dependences on the trigger PMT ADC bin center are shown for one, two, and three fiber readout with closed squares, upward closed

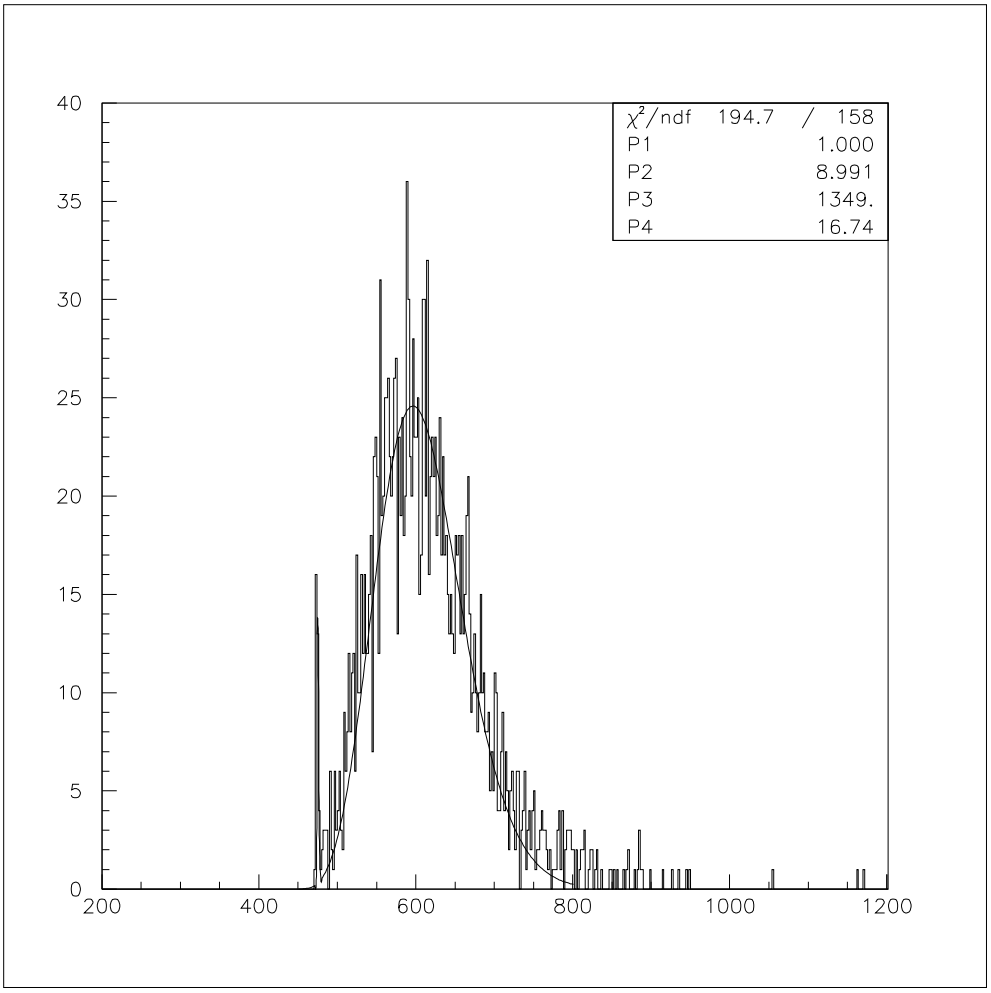

Figure 16: Fit to the test PMT ADC spectrum corresponding to trigger PMT ADC range from 700 to 1500. The average number of photo-electron is ~ 9.

triangles, and downward closed triangle, respectively. Source (^{90}Sr) position was unchanged during these measurements. As one can see the number of photo-electrons is proportional to the number of fibers. In the figure the open squares represent the χ^2 distribution for the fit to two fiber readout case.

Source position dependence was studied using three fiber readout. Source was moved on the surface of the strip from one side to another and the measurements of the light yield were performed at four points. The results are shown in Fig. 18. No dependence on the position of the source is observed. However, it should be noted that the multi fiber readout and the position

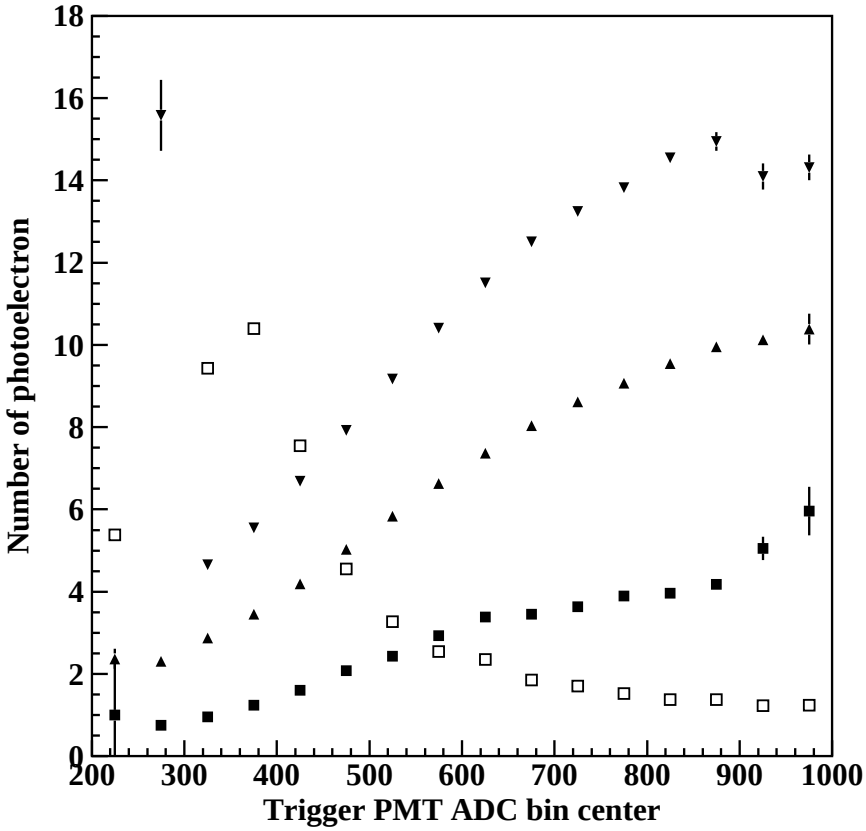

Figure 17: Dependence of the n_{pe}'s on the trigger PMT ADC channel for one (closed squares), two (closed upward triangles), and three (closed downward triangles) WLS fiber readout from Kharkov scintillator strip with three grooves on the surface. Radiative source was ^{90}Sr and the readout PMT was the R6095. The open squares the χ^2 distributions for the fit to two fiber readout case.

dependence should be checked with final strip geometry, since the Kharkov scintillators are only 2.63 cm wide, while for the pre-shower 4.5 cm wide scintillators will be used.

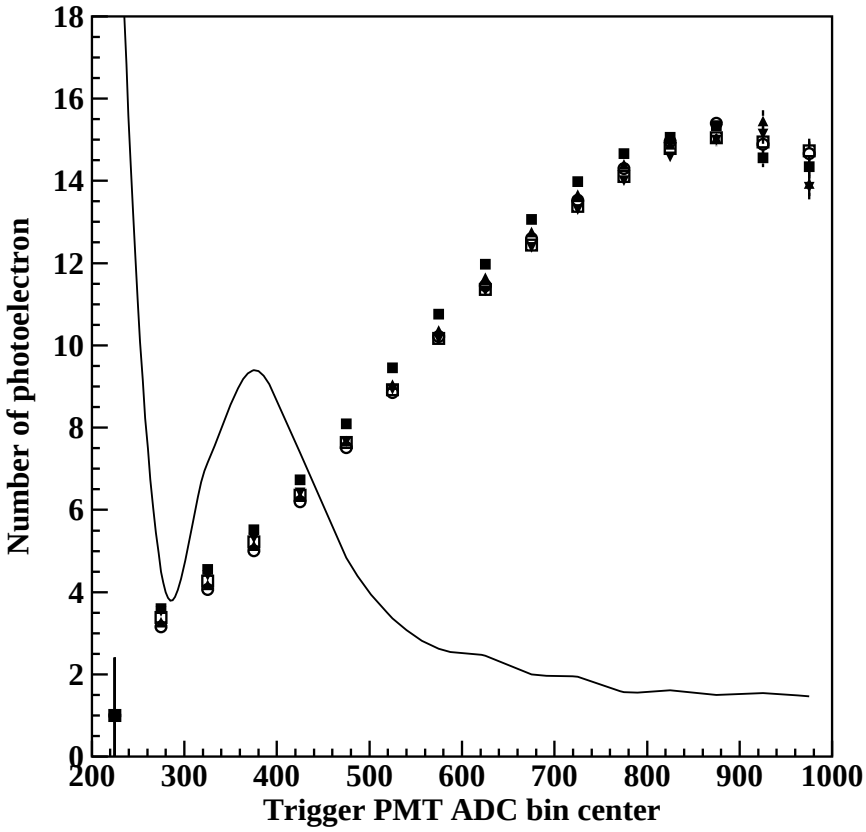

Figure 18: Dependence of the n_{pe}s on the trigger PMT ADC channel for three fiber readout of Kharkov three groove scintillator strip. Different color symbols correspond to different position of the ^{90}Sr radiative source. For light readout R6095 PMT was used.

7 Summary

Light yield for several different types of scintillator strips, WLS green fibers, and PMTs were measured. The purpose of these measurements were to select the best combination of the scintillator-WLSF-PMT based on the performance and price. Systematic uncertainties of the relative light yield measurements of different combinations of scintillator-WLSF-PMT were $<$ 10%. For the absolute light yield, the estimated systematic error was $\sim$ 20%.

The best results were obtained with the FNAL extruded scintillator, KURARAY Y11 fibers, and the HAMAMATSU R7899EG PMT. The HAMAMATSU PMT R6095, selected with QE $>$ 16% at 500 nm, showed only $\sim$ 25% less light yield, while in price it is about 1.5 times less expensive. Multi-clad fiber readout showed $\sim$ 20% more light than a single clad fiber, but it is about 35% more exspensive.

Based on the measurements results and the available price estimates, the choice for the pre-shower will be: the FNAL extruded scintillator, KURARAY 1 mm diameter, single clad Y11 fiber, and the HAMAMATSU R6095 PMT, selected with QE $>$ 16% at 500 nm. It should be notted that by the performance and price, extruded scintillators from Amcrys-Plast, Kharkov (Ukraine), wave-length shifting fibers G91A from BICRON and the HAMAMATSU PMT R1450, selected to have $>$ 18% quantum efficiency at 500 nm, were not too far from the best choice set and generally meet the requirements for the pre-shower.

References

[1] M. Amarian *et al.*, NIM **A 460**, 239 (2001),

[2] N. Dashyan *et al.*, CLAS-NOTE 2007-001 (2007).

[3] S. Stepanyan *et al.*, CLAS-NOTE 2002-001 (2002).

[4] MINOS Far detector, arXiv:hep-ex/0507018 (2005).

[5] FNAL Extruder http://www.nicadd.niu.edu/research/extruder.

[6] M. Amarian *et al.*, CLAS-NOTE 1992-012 (1992).

[7] V. Burkert *et al.*, CLAS-NOTE 1992-008 (1992).

[8] K. Giovanetti and A. Stavola, Fiber adapters for pre-shower tests (JMU).

[9] HBOOK, Statistical Analysis and Histogramming, CERN program library long write-ups Y250.

[10] Physics Analysis Workstation, CERN program library long write-ups Q121.